IOSR Journal of Applied Chemistry (IOSR-JAC)
ISSN: 2278-5736
PP 41-50
www.iosrjournals.org

Influence of Palladium Loading on the Degradation Property of TitaniaNanostructures

SuprabhaT[1], Suresh Mathew[2]
[1](*Department of Science, Sree Narayana Gurukulam College of Engineering, Kadayiruppu, Kerala, India)*
[2](*Advanced Molecular Materials Research Centre, Mahatma Gandhi University, Kottayam, Kerala, India)*

ABSTRACT: *The influence of palladium loading on titania nanostructures with three different morphologies viz., cubes, spheres and rods was studied. Nanotitania was synthesized by microwave irradiation method. Nano-sized palladium particles were loaded on synthesized titania nanostructures by metal sol method. As-synthesized TiO_2 and Pd-TiO_2 were characterized by XRD, UV-visible spectroscopy, BET surface area, PLand TEM techniques. Photocatalytic degradation property of titania and palladium loaded titania nanostructures were investigated using the dye methylene blue under sunlight. The dye degradation capabilitiesof nano-sized Pd-TiO_2catalysts were found superior to bare TiO_2 nanostructures. The higher photoactivity of Pd-TiO_2 can be ascribed to the effect of enhancement of electron hole separation by the Pd deposits acting as electron traps on the TiO_2 surface.*
Key words: *Dye degradation, microwave irradiation, photocatalysis, Pd-TiO_2, titania.*

I. Introduction

Many photocatalysts have been attempted for the degradation of pollutants in wastewater. Among the semiconductors employed, titanium dioxide has generated intensive interest for its semiconducting and photocatalytic properties [1-4]. It is environmentally benignand relatively inexpensive with unique electronic and optical properties. It also exhibits long-term stability against photo and chemical corrosion[5]. It has also been applied to inactivate bacteria, viruses, and cancer cells [6-7].

There are a few drawbacks associated with the use of TiO_2.It has a high bandgap (Eg> 3.0 eV) and it is excited only by UV light (λ < 400 nm) to inject electrons into the conduction band and to leave holes into the valence band. Thus, this practically limits the use of sunlight or visible light as an irradiation source in photocatalytic reactions on TiO_2.Numerous studies have been recently performed to enhance electron–hole separation and to extend the absorption range of TiO_2 into the visible range. These studies include doping metal ions into the TiO_2 lattice, addition of inert support and deposition of noble metals [8-18].

We have already reported a simple microwave method to synthesize phase pure anatase and rutile nanotitania with different morphologies *viz*., cubes, spheres and rods[19]. Au and Ag loaded titania nanostructures were prepared to investigate the effect of both physical and chemical characteristics of the catalyst together with their influence on the photocatalytic activity of TiO_2 towards the photocatalytic degradation of methylene blue. Au and Ag loaded TiO_2 showed higher photocatalytic activity compared to bare TiO_2 and shifted the absorption into visible region[20,21]. In the present work, we could enhance the visible light photocatalysis of titania nanostructures by loading platinum by metal sol method [22]. In the present work, we report the influence of palladium loading on the degradation property oftitania nanostructures.To the best of our knowledge no one has reported previously the preparation of Pd loaded TiO_2 using TiO_2synthesized by microwave irradiation technique. By applying microwave heating, the reaction mixture is heated rapidly and more uniformly through direct molecular interaction with electromagnetic radiation. This technique would also reduce reaction time and gives better yield. The major advantages of using microwaves are rapid heat transfer and selective heating [23-24]. The catalytic performances of morphologically different three crystalline nanotitania and their palladium loaded structures (Pd/TiO_2) were studied for dye degradation of methylene blue under sunlight.

II. Experimental Details

2.1. Materials

All reagents were purchased from Merck, Germany. Titanium trichloride (15 wt. % TiCl3, 10 wt. % HC1) was used as the titanium precursor. NH4OH (1.5 M), NaCl (5 M) and NH4Cl (5 M), PdCl2, NaBH4, and polyvinyl alcohol (PVA) were employed for the synthesis. Commercially available TiO2 (P-25) from Degussa (Germany) consists of 70% anatase and 30% rutile with a specific BET surface area of 50 m2 g-1 and having

particle size of 30 nm was used throughout the experiments. A typical microwave oven (Whirlpool, 1200 W) operating at a frequency of 2450 MHz was used for the synthesis. All chemicals were of reagent-grade quality and were used as received.

2.2. Synthesis of Pd loaded TiO2 nanostructures

The TiO2 nanostructures having cubical (S1), spherical (S2) and rod like (S3) morphology were synthesized as in our early report[19] and were loaded with 0.5 wt %Pd using metal sol method. For this a suitable amount of PVA solution (1 wt %) was added to an aqueous PdCl2 solution (0.1 mg Pd/ml) under vigorous stirring. Then, a freshly prepared solution of NaBH4 (molar ratio NaBH4/Pd = 4) was slowly added dropwise into the mixture. The TiO2 samples were added after the pH was adjusted to 6.0 by NH4OH or HCl solution. The mixture was stirred at 60^{o}C for 3 hrs, then filtered and washed until no Cl- was detected by AgNO3 solution. After being dried at 100^{o}C overnight, the samples were calcined at 550 ^{o} C in air for 4 hrs. The Pd loaded on samples S1, S2 and S3 are represented as PdS1, PdS2 and PdS3 respectively.

2.3. Characterization of Pd loaded and pure Titania Nanostructures

The X-ray diffraction (XRD) patterns of the titania were recorded on a Brucker D8 advance diffractometer with CuKα radiation. The crystallite size of TiO2 was calculated using Debye Scherrer equation, $L = k\lambda/(ß \cos\theta)$, where L is the average crystallite size, λ is the wavelength of the radiation, θ is the Bragg's angle of diffraction, ß is the full width at half maximum intensity of the peak and k is a constant usually applied as 0.89. High resolution transmission electron micrographs and electron diffraction patterns were recorded using a JEOL JEM-3010 HRTEM microscope at an accelerating voltage of 300 kV. The TEM specimens were prepared by drop casting the sample on the surface of the carbon coated copper grid. The BET surface area, pore size distribution and pore volume of the samples were measured on a Micromeritics ASAP 2010 analyzer based on N2 adsorption at 77 K in the pressure range from 0.1 to 760 mm Hg. The ultraviolet–visible absorption (UV–vis) spectra were recorded using a UV-2450 Shimadzu UV–visible spectrophotometer. The photoluminescence (PL) spectral measurements were made using Perkin Elmer LS-55 luminescence spectrometer at an excitation wavelength of 325 nm.

2.4. Photocatalytic Activity Measurements

Photocatalytic activity of TiO_2 was evaluated by the degradation of the dye, methylene blue (MB) in aqueous solution under sunlight in the presence of as-synthesized TiO_2 and the Pd loaded TiO_2. The changes in the concentrations of methylene blue in the aqueous solution were examined by absorption spectra measured on a UV-2450 Shimadzu UV–visible spectrophotometer. Before examining the photocatalytic activity for degradation of aqueous methylene blue, TiO_2 and Pd/TiO_2 sol was prepared. About 100 mg of the synthesized TiO_2 or Pd/TiO_2 was dispersed ultrasonically in 100 ml of 4 □ 10^5 M methylene blue solution in a quartz reactor. To maximize the adsorption of the dye onto the TiO_2 surface, the resulting mixture was kept in the dark for 30 min under stirring conditions[25].The degradation of the dye was monitored by measuring the absorption maximum of methylene blue at 661 nm at 30 min intervals of reaction.

III. Results and Discussion

3.1. X-ray Diffraction Studies

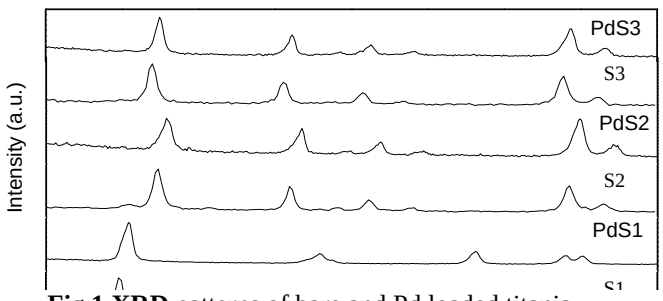

Fig.1 XRD patterns of bare and Pd loaded titania

The X-ray diffraction (XRD) patterns (Fig. 1) of the TiO_2 particles show that anatase phase with lattice constants, a = 3.777 and c = 9.501 was formed (JCPDS file no. 89-4921) in NH_4OH medium (S1). All the peaks in S2 (NaCl medium) and S3 (NH_4Cl medium) correspond to rutile phase with lattice constants a = 4.608, c = 2.973 and a = 4.548, c = 2.946, respectively (JCPDS files, no. 76-0319 and 88-1173).It is clear from the fig.1 that all the samples are highly crystalline and phase pure. It is also observed that there is no phase change due to palladium loading on the samples S1, S2 and S3. Further, no palladium peaks were found in the XRD patterns. The average crystallite sizes of S1, S2, S3, PdS1, PdS2 and PdS3 are 12, 10, 21, 11, 10 and 20 nm respectively.On palladium loading the average crystallite sizes decreased slightly[26]. The X-ray diffraction patterns of palladium loaded TiO_2 samples almost coincide with that of bare TiO_2 showing no diffraction peaks due to palladium species thus suggesting that the metal particles are well dispersed on the TiO_2 surface[27]. This result can presumably be due to a combination of factors namely low Pd contents for loading, small particle size and homogeneous particle distribution[28-29]. X-ray diffractograms (Fig. 1) shows that on Pd loading, there is a slight shift of the peak to the higher angle indicating a slight decrease in the d spacing. This is consistent with d value obtained from TEM analysis.

3.2. BET Surface Area Analysis

The crystallite size, BET surface area, pore size, and pore volume values are summarized in Table 1. The surface area of S1, S2, and S3 are 96, 77, and 34 $m^2 g^{-1}$, respectively. The sample S1 has highest surface area and is due to its mesoporous nature with pore size around 4 nm. Palladium loaded TiO_2 particles show a decrease in surface area of the samples as is evident from the table and this can be ascribed to the calcination process used during the synthesis. The decrease in surface area after palladium loading is appreciable in the case of S1. This may be due to the blocking of pores on the TiO_2nanocube surface by palladium particles.

3.3. Microscopic Analysis

Table 1 The crystallite size, BET surface area, pore size, and pore volume values of bare and Pd loaded TiO_2 samples

Sample code	Crystallite size from XRD (nm)	BET surface area (m^2g^{-1})	Pore size (nm)	Pore volume ($cm^3 g^{-1}$)
S1	12	96	4	0.37
S2	10	77	2.5	0.18
S3	21	34	2.0	0.10
PdS1	11	76	2.5	0.29
PdS2	10	65	1.7	0.12
PdS3	20	33	1.2	0.10

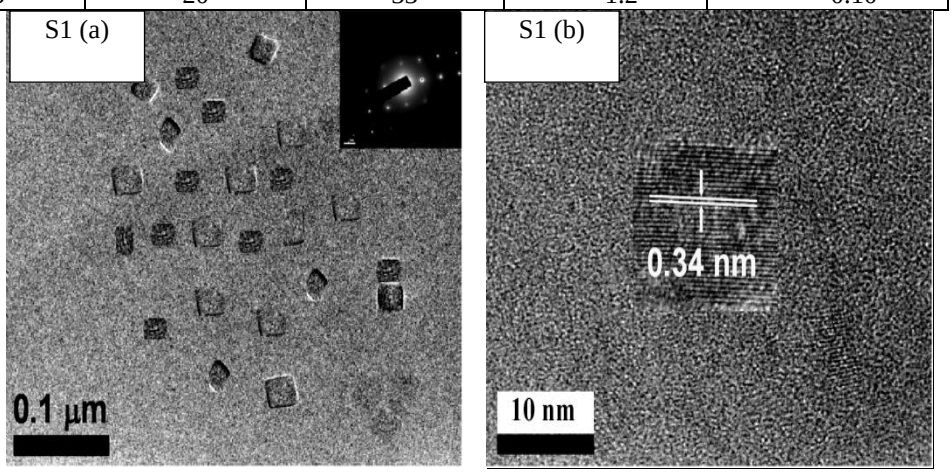

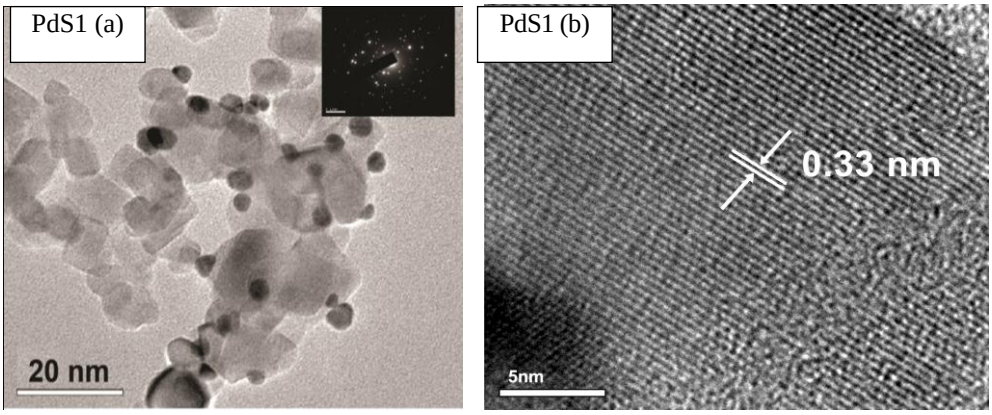

Fig. 2. a. HRTEM of bare and palladium loaded TiO_2 (S1 and PdS1)

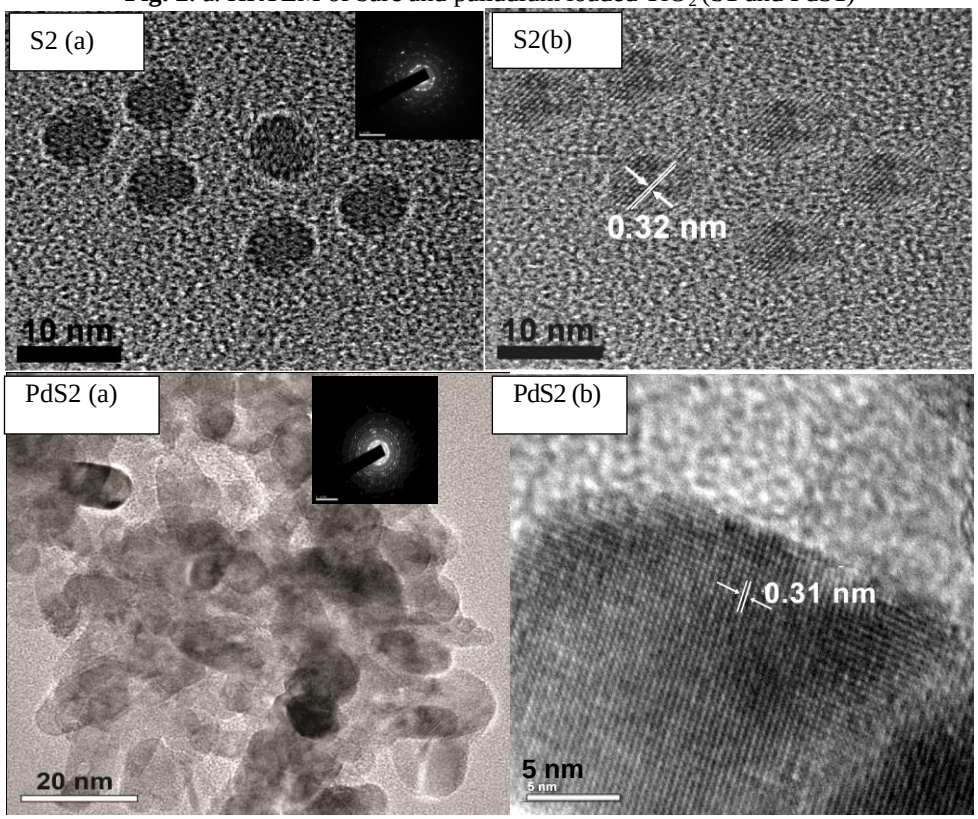

Fig. 2. b. HRTEM of bare and palladium loaded TiO_2 (S2 and PdS2)

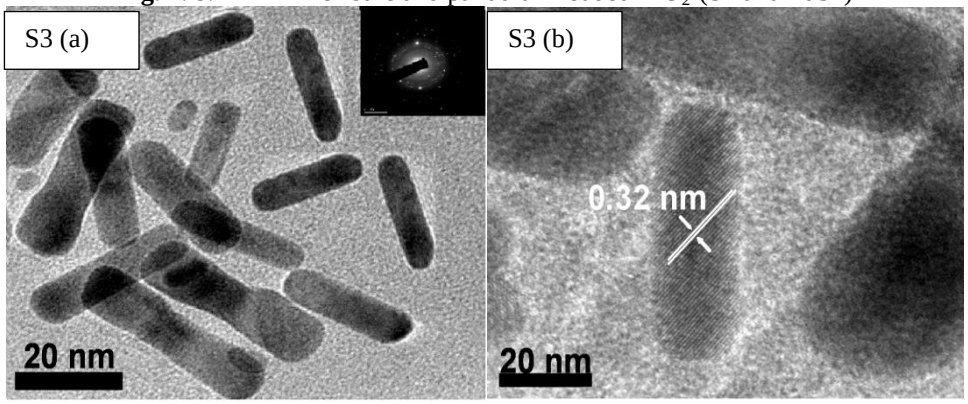

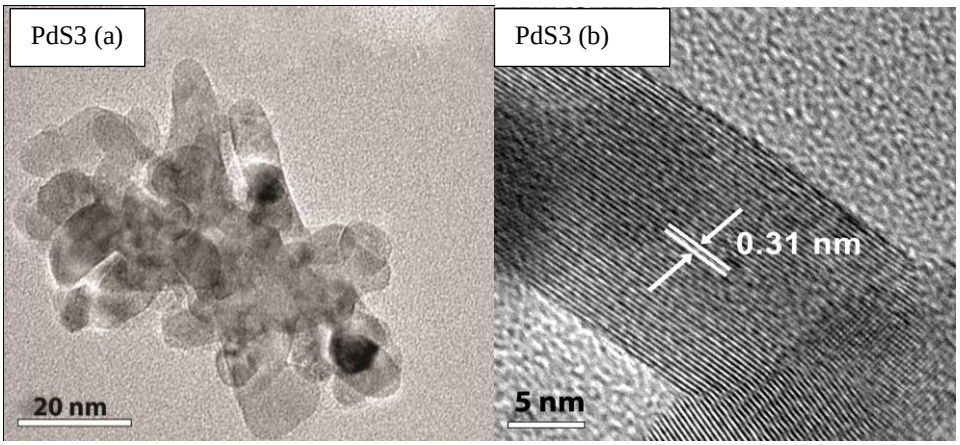

Fig. 2. c. HRTEM of bare and palladium loaded TiO_2 (S3 and PdS3)

The HRTEM images of the bare and palladium loaded TiO_2 nanoparticles synthesized are shown in Fig. 2. TEM images of S1 (a) and PdS1 (a) shows the formation of nanocubes with particle size around 25 nm with pores. The HRTEM image of S1 (b) shows lattice fringes of the anatase phase with d = 0.34 nm and PdS1 (b) shows lattice fringes of the anatase phase with d = 0.31 nm. The selected area electron diffraction pattern in the inset of the S1 (a) and PdS1 (a) confirms that the sample S1 is a single crystalline anatase phase. The high surface area observed for the sample S1 and PdS1 may be due to the highly porous nature of the cubes. Sample S2 (a) and PdS2 (a) shows the formation of nanospheres with average size around 8 nm. Corresponding selected area electron diffraction pattern of S2 and PdS2 are shown in the inset. The pattern indicates the polycrystalline nature of the sample. Lattice image of S2 (b) of these nanospheres shows lattice fringes of the rutile phase with d = 0.32 nm and lattice image of PdS2 (b) shows lattice fringes of the rutile phase with d = 0.31 nm. S3 (a) and PdS3 (a) shows the formation of nanorods with an average aspect ratio of around 4 nm. Corresponding SAED pattern indicates a polycrystalline nature, which may be due to the diffraction in a bunch of nanorods. The HRTEM image of nanorod S3 (b) shows clear lattice fringes of the rutile phase with d = 0.32 nm and PdS3 (b) shows lattice fringes of the rutile phase with d = 0.31 nm. In all the three Pd loaded samples d spacing has decreased and can be ascribed to the effect of occupation of Pd particles in the lattice. Pd loaded samples showed the presence of very small, spherical and well dispersed palladium nanoparticles on the TiO_2 surface and it appears as black spots in Fig. 4 (PdS1(a), PdS2(a) and PdS3(a)).

3.4. UV–Visible Absorption Studies

Fig.3 shows the UV-vis absorption spectra of titania nanostructures S1, S2, and S3. The onset of absorption for the three samples is 382, 405, and 415 nm for S1, S2 and S3, respectively.

The broad absorbance band in 450-550 nm regions in the palladium loaded samples PdS1, PdS2 and PdS3 corresponds to the well reported plasmon resonance of nanopalladium particles[30].

It is clear from the fig.3 that palladium loaded samples showed significant absorption in the visible region. The red shifted photoresponse of these samples may lead to high photocatalytic activity under visible region which helps in the enhancement of photocatalytic activity under sunlight. The band gap energies were calculated using the equation[30]

$$Eg = 1239.8/\lambda$$

whereEg is the band gap (eV) and λ (nm) is the wavelength of the absorption edges in the spectrum.

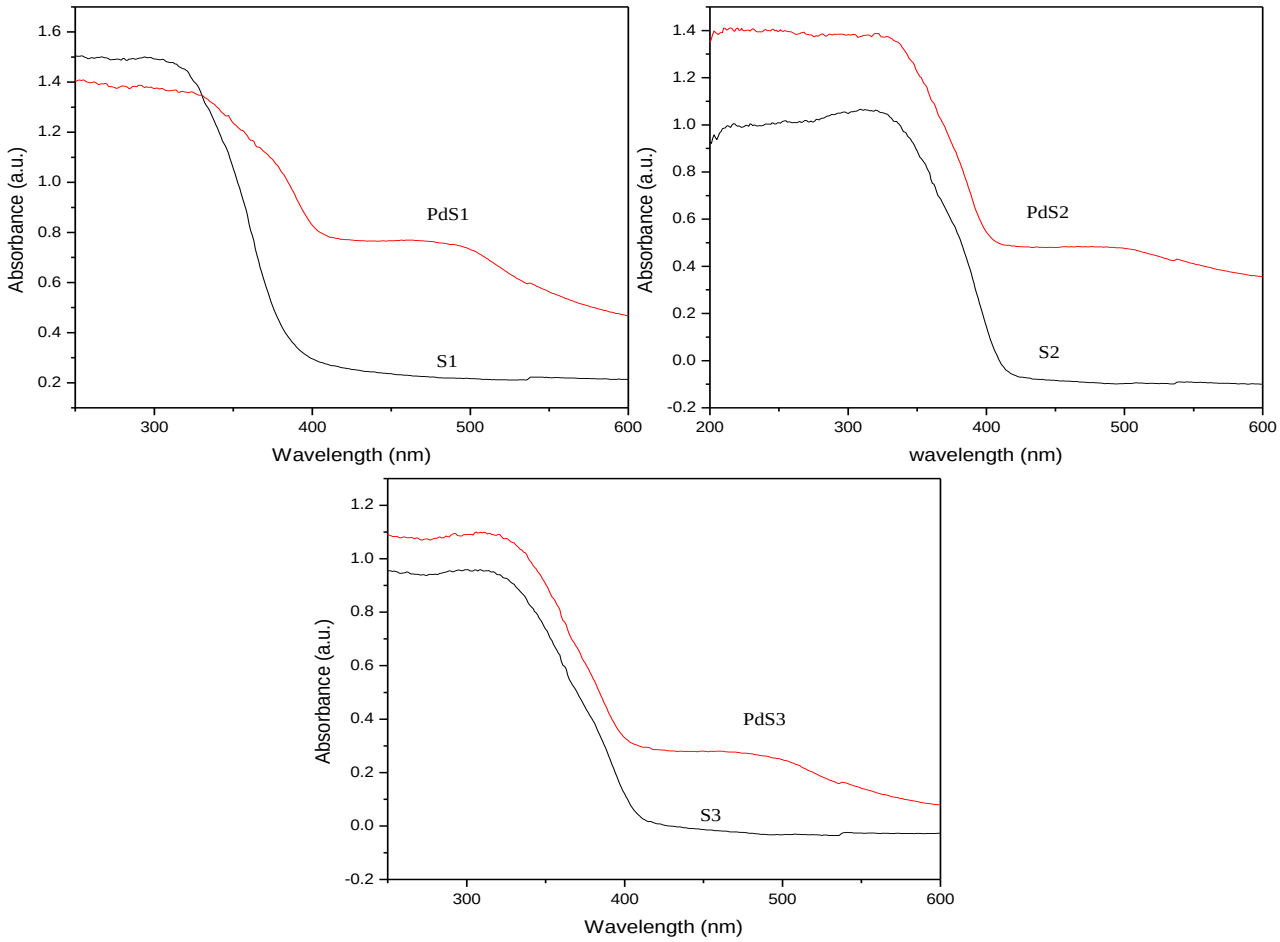

Fig. 3 UV–visible absorption spectra of bare and palladium loaded TiO_2

Table 2 Band gap values of bare and Pd loaded nano TiO_2

Sample	Band gap (eV)
S1	3.2
S2	3.17
S3	3.15
PdS1	2.95
PdS2	2.89
PdS3	2.91

The band gap values of bare and palladium loaded nanotitania samples are given in Table 2. The band gap energy of nanocubes (S1, 3.2 eV) is significantly higher as compared to that of nanospheres (S2, 3.17 eV) and nanorods (S3, 3.15 eV). For anatase, the band gap (Eg) is estimated to be 3.2 eV, which is in good agreement with the reported value for anatase (3.2–3.3 eV). The absorption spectrum of rutile shows a lower absorption and the calculated band gap is around 3.17 and 3.15 eV respectively for the nanostructures S2 and S3. However, rutile nanostructures show a slightly higher band gap than the reported value (3.0–3.1 eV). The higher band gap may be due to the smaller particle size. The band gap values of palladium loaded TiO_2 samples are less than that of bare titania nanostructures (Table 2). The lower band gap of palladium loaded TiO_2 can enhance the photocatalytic activity of these samples under visible light.

3.5. Photoluminescence Studies

The photoluminescence emission spectra (PL) of bare and palladium loaded TiO_2 samples were studied in the range of 250-700 nm to investigate the separation efficiency of charge carriers and the results are shown in Fig. 4.

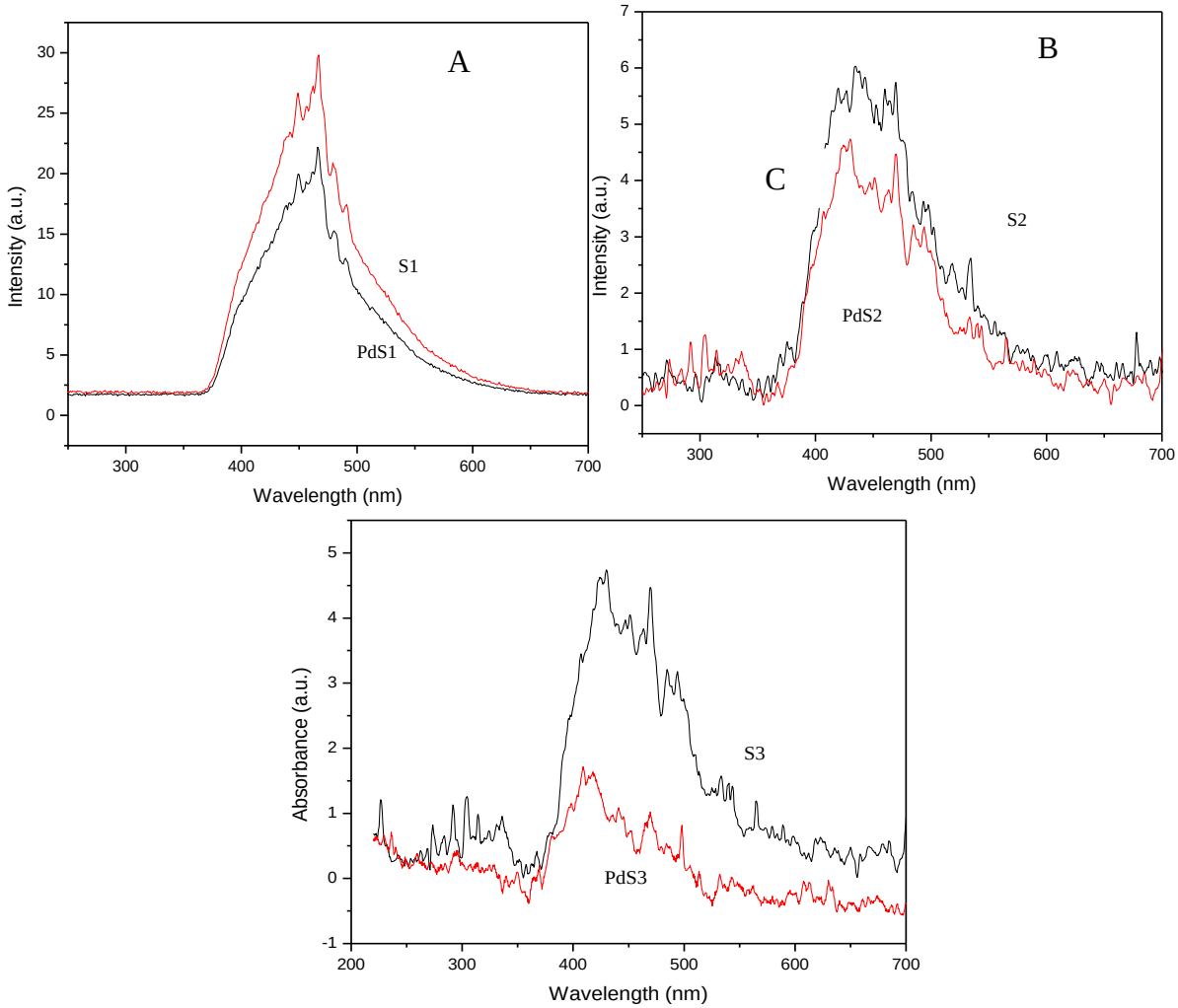

Fig. 4 The photoluminescence emission spectra (PL) of bare and palladium loaded TiO_2

It is evident from the fig.4 that the PL intensity of TiO_2 was decreased with palladium loading. The lower PL intensity shows that the rate of recombination between electrons and holes are low[31,32]. The electrons are excited from valence band (VB) to conduction band (CB) of TiO_2 under UV irradiation and generate photoexcited electrons and holes. Although loading with palladium narrows the band gap of TiO_2 samples, the recombination of electrons and holes are relatively slow which is evident from PL spectra.

For palladium loaded TiO_2 samples, palladium plays an important role in the interfacial charge transfer and in the decrease in rate of electron-hole recombination. Palladium particles could act as an effective electron scavenger to trap the photo induced electrons and holes of TiO_2 leading to the reduction of electron–hole recombination and thus improving the photocatalytic efficiency. The decrease in PL intensity of palladium loaded samples is in the order PdS1>PdS2>PdS3 as is evident from the fig.4 which indicates that the electron – hole recombination is less for PdS1 than PdS2 and PdS3. This also helps for the higher photocatalytic activity of PdS1 than PdS2 which in turn greater than PdS3. The electrons trapped in palladium sites were subsequentlytransferred to the surrounding adsorbed O_2. PL emission spectra studies have been widely used to investigate the fate of electron hole pairs in semiconductor particles, since PL emission results from the recombination of free carriers[31,32]

3.6. Photocatalytic activity

To investigate the photocatalytic activity of synthesized TiO_2 samples in solar light, the degradation of methylene blue was studied in presence of bare and palladium loaded TiO_2 nanoparticles under sunlight. For comparison, photocatalytic studies were also performed with commercially available photocatalyst, Degussa P25 and the results are depicted in Fig. 5.

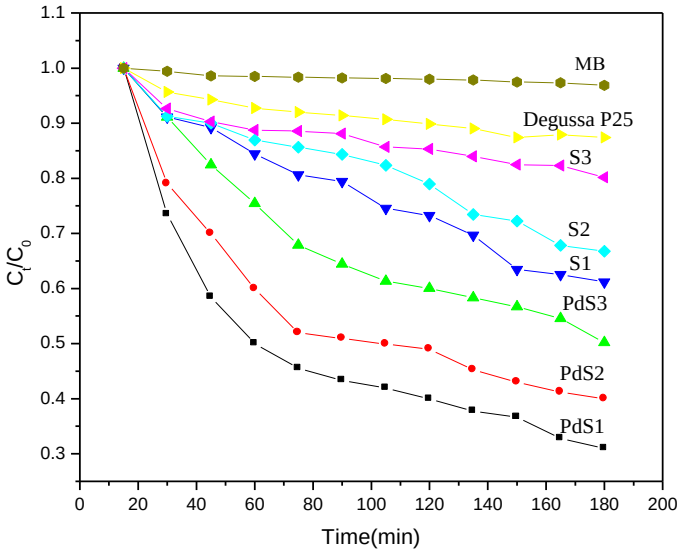

Fig. 5 Photocatalytic activity of bare and palladium loaded TiO_2 samples in solar light

Methylene blue (MB) shows a maximum absorption at 661 nm. The absorption peak gradually diminishes upon solar light irradiation, illustrating the methylene blue degradation. It is clear that the anatasetitanianananocubes (S1) shows higher photocatalytic activity than the other two rutile nanostructures (S2 and S3) as we reported earlier [20]. The difference in activity of the synthesized samples is related to their surface area, particle size and phase. Small crystallite size and mesoporous texture produces high surface area TiO_2 and can provide more active sites and adsorb more reactive species. S1 is purely anatase phase and has the highest surface area among the three samples, it exhibits the highest photocatalytic activity. The appreciable activity observed for the nanorods (34 m^2 g^{-1}) compared to Degussa P25 (50 m^2 g^{-1}) is due to the preferentially grown 110 planes in the nanorod morphology as reported in our paper[20]. The activity of different samples in sunlight is in the order PdS1> PdS2 > PdS3 >S1 > S2 >S3 > Degussa P25.The high activity of palladium loaded TiO_2 than corresponding bare titania nanostructures is mainly attributed to the decrease in band gap so that visible light is enough to excite electrons from valence band to conduction band.

IV. Conclusions

Anatasenanocubes (S1), rutile nanospheres (S2) and rutile nanorods (S3) were synthesized using a simple microwave irradiation technique by changing the pH of the media. The synthesized titania nanostructures were loaded with palladium in order to improve the photocatalytic activity of the samples under visible region. Structural and physicochemical characterization revealed the dependence of photocatalytic activity with different morphologies. Among bare samples, anatasenanocubes (S1) exhibit a much higher BET specific surface area than rutile nanospheres (S2) and nanorods (S3). The band gap energy for anatase nanocubes is greater than that of the rutile nanospheres (S2) and nanorods (S3). Loading of palladium particles could improve the photocatalytic properties of the titania nanostructures under sunlight. Among the various titania nanostructures, Pd-loaded titanianananocubes exhibit enhanced photocatalytic activity compared to Pd-loaded titanianananospheres and nanorods.

Acknowledgements

Financial support from the University Grants Commission (UGC), New Delhi by way of the FIP programme to Suprabha T is gratefully acknowledged.

References

[1]. D. M. Tobaldi, C. Piccirillo,R. C. Pullar, A. F. Gualtieri, M. P. Seabra, P. M. L. Castro, and J. A. Labrincha, Silver-Modified Nano-titania as an Antibacterial Agent and Photocatalyst, The Journal of Physical Chemistry C 118, 2014, 4751-4756.

[2]. X. Zheng , S. Meng , J. Chen , J. Wang , J. Xian , Y. Shao, X. Fu, and D. Li, Titanium dioxide photonic crystals with enhanced photocatalytic activity: matching photonic band gaps of TiO2 to the absorption peaks of dyes, The Journal of Physical Chemistry C. 117, 2013, 21263−21273.

[3]. K. Balachandran, R. Sivaraj, and R. Venckatesh, Removal of Methylene Blue Using Prepared Nano Titanium Dioxide (TiO2) Photocatalyst, J. Environ. Nanotechnol., 2(1), 2013, 12-15.

[4]. X. B. Ren, M. Chen, and D. J. Qian,Pd (II)-Mediated Triad Multilayers with Zinc Tetrapyridylporphyrin and Pyridine-Functionalized Nano-TiO2 as Linkers: Assembly, Characterization, and Photocatalytic Properties, Langmuir, 28, 2012, 7711-19 .

[5]. Y. Shiraishi, Y. Takeda, Y. Sugano, S. Ichikawa, S. Tanaka, and T. Hirai, Highly efficient photocatalytic dehalogenation of organic halides on TiO2 loaded with bimetallic Pd-Pt alloy nanoparticles, Chem. Commun. 47, 2011, 7863-7871.

[6]. A. Mukhopadhyay, S. Basak, J. K. Das, S. K. Medda, K. Chattopadhyay, and G. De, Ag-TiO2 Nanoparticle Codoped SiO2 Films on ZrO2 Barrier-Coated Glass Substrates with Antibacterial Activity in Ambient Condition, ACS Appl. Mater. Interfaces 2, 2010, 2540-2546.

[7]. Y. Liu, Q. Li, J. Zhang, W. Sun, S. Gao, and J. K. Shang, PdO loaded TiO2 hollow sphere composite photocatalyst with a high photocatalytic disinfection efficiency on bacteria, Chemical Engineering Journal, 249 (1), 2014, 63-71.

[8]. N. Hintsho, L. Petrik, A. Nechaev, S. Titinchi, and P. Ndungu , Photo-catalytic activity of titanium dioxide carbon nanotube nano-composites modified with silver and palladium nanoparticles, Applied Catalysis B: Environmental, 156, 2014, 273-283.

[9]. P. Sangpour, F. Hashemi, and A. Z. Moshfegh, Photoenhanced Degradation of Methylene Blue on Cosputtered M: TiO_2 (M) Au, Ag, Cu) Nanocomposite Systems: A Comparative Study, J. Phys. Chem. C, 114, 2010, 13955-13961.

[10]. W. Xu, S. Zhu, Z. Li, Z. Cui, and X. Yang, Synthesis and catalytic properties of Pd nanoparticles loaded nanoporous TiO_2 material, Electrochimica Acta, 114, 2013, 35-41.

[11]. N. Zhang, S. Liu, X. Fu, and Y. Xu, Synthesis of M@TiO_2 (M = Au, Pd, Pt) Core Shell Nanocomposites with Tunable Photoreactivity, J. Phys. Chem. C115, 2011, 9136-9145.

[12]. A. Z. Jurek , and J. Hupka, Preparation and characterization of Pt/Pd-modified titanium dioxide nanoparticles for visible light irradiation Catalysis Today, 230, 2014, 181-187.

[13]. H. S. M. Tabaei, M. Kazemeini, and M. Fattahi, Preparation and characterization of visible light sensitive nano titanium dioxide photocatalyst, Scientia Iranica,19 (6), 2012, 1626-1631.

[14]. J. Kim, P. Zhang, J. Li, J. Wang, and P. Fu, Photocatalytic degradation of gaseous toluene and ozone under UV254+185 nm irradiation using a Pd-deposited TiO_2 film, Chemical Engineering Journal, 252, 2014, 337-345.

[15]. L. Han, Y. Xin, H. Liu,X. Ma, and G.Tang, Photoelectrocatalytic properties of nitrogen doped TiO2/Ti photoelectrode prepared by plasma based ion implantation under visible light, Journal of Hazardous Materials, 175(1-3), 2010, 524-531.

[16]. J. C. S. Wu, and C. H. Chen, A visible-light response vanadium doped titania nano catalyst by sol-gel method, Journal of Photochemistry and Photobiology A: Chemistry, 163 (3), 2004, 509-515.

[17]. J. Thomas, K. P. Kumar, and S. Mathew, Hydrothermal Synthesis of Samarium Doped Nanotitania as Highly Efficient Solar Photocatalyst. Science of Advanced Materials, 2(4), 2010, 481–488.

[18]. M. Yamauchi, R. Abe, T. Tsukuda, K. Kato, and M. Takata, Highly selective ammonia synthesis from nitrate with photocatalytically generated hydrogen on CuPd/ TiO2. J. Am. Chem. Soc. 133, 1150-1152.

[19]. T. Suprabha, H. G. Roy, J. Thomas, K. P. Kumar, and S. Mathew, Microwave-Assisted Synthesis of Titania Nanocubes, Nanospheres and Nanorods for Photocatalytic Dye Degradation., NanoscaleRes.Lett.4, 2009, 144 -152.

[20]. T. Suprabha, H. G. Roy, and S. Mathew, Gold Loaded Titania Nanostructures - Synthesis, Characterization and Morphology Dependence on Photocatalysis, Sci. Adv. Mater. 2, 2010, 107-114.

[21]. T. Suprabha, H. G. Roy, and S. Mathew, Silver Loaded Titania Nanostructures with Extended Spectral Response for Enhanced Solar Photocatalysis, J. Nanoscience Letters 2, 2012, 19-26.

[22]. J. D. Grunwaldt , C. Kiener , C . Wogerbauer, and A. Baiker, Preparation of Supported Gold Catalysts for Low-Temperature CO Oxidation via Size-Controlled Gold Colloids. Journal of Catalysis,181,2,1999, 223-232.

[23]. M. I. Dar, A. K. Chandiran , M. Gr¨atzel, M. K. Nazeeruddin, and S. A. Shivashankar, Controlled synthesis of TiO_2 nanoparticles and nanospheres using a microwave assisted approach for their application in dye-sensitized solar cells, Journal of Materials Chemistry A. 2, 2014, 1662–1667.

[24]. Y. Yang, G. Wang, Q. Deng, D. H. L. Ng, and H. Zhao, Microwave-Assisted Fabrication of Nanoparticulate TiO_2 Microspheres for Synergistic Photocatalytic Removal of Cr(VI) and Methyl Orange, ACS Appl. Mater. Interfaces. 6, 2014, 3008 -15.

[25]. D. Zhang, D. Yang, H. Zhang, C. Lu, and L. Qi, Synthesis and Photocatalytic Properties of Hollow Microparticles of Titania and Titania/Carbon Composites Templated by Sephadex G-100, Chem. Mater. 18(15), 2006, 3477 -3485.

[26]. S. H. Nam, H. S. Shim, Y. S. Kim, M. A. Dar, J. G. Kim, and W. B. Kim, Ag or Au Nanoparticle-Embedded One-Dimensional Composite TiO_2 Nanofibers Prepared via Electrospinning for Use in Lithium-Ion Batteries, ACS Appl. Mater. Interfaces, 2(7), 2010, 2046-2052.

[27]. A. A. Ismail, D. W. Bahnemann, L. Robben, V. Yarovyi, and M. Wark, Palladium Doped Porous Titania Photocatalysts: Impact of Mesoporous Order and Crystallinity, Chem.Mater. 22(1), 2010, 108-116.

[28]. I. Nakamura, N. Negishi, S. Kutsuna, T. Ihara, S. Sugihara, and K. Takeuchi, Role of oxygen vacancy in the plasma-treated TiO_2 photocatalyst with visible light activity for NO removal. Journal of Molecular Catalysis A: Chemical. 161(1-2), 2000, 205–212.

[29]. V. Polshettiwar, and R. S. Varma. Microwave-assisted organic synthesis and transformations using benign reaction media, Accounts of Chemical Research, 41(5), 2008, 629-639.

[30]. S. F. Chen, J. P. Li, K. Qian, W. P. Xu, Y. Lu, W. X. Huang, and S. H. Yu, Large scale photochemical synthesis of M@ TiO_2 nanocomposites (M = Ag, Pd, Au, Pt) and their optical properties, CO oxidation performance and antibacterial effect, Nano Res. 3, 2010, 244-255

[31]. Y. Cong, J. Zhang, F. Chen, M. Anpo, and D. He, Preparation, Photocatalytic Activity,and Mechanism of Nano-TiO_2 Co-Doped with Nitrogen and Iron (III) J. Phys. Chem. 28, 2007,10618-10623.

[32]. F. B. Li, X. Z. Li, M. F. Hou, K. W. Cheah, and W. C. H. Choy, Enhanced photocatalytic activity of Ce^{3+}– TiO_2 for 2-mercaptobenzothiazole degradation in aqueous suspension for odour control, Applied Catalysis A: General, 285(1-2), 2005, 181-185.